HHS Public Access

Author manuscript

J Clin Neurophysiol. Author manuscript; available in PMC 2024 February 01.

Published in final edited form as:

J Clin Neurophysiol. 2023 February 01; 40(2): 144–150. doi:10.1097/WNP.0000000000000867.

Manifestation of hippocampal interictal discharges on clinical scalp EEG recordings

Somin Lee[1,2], **Shasha Wu**[3], **James X. Tao**[3], **Sandra Rose**[3], **Peter C. Warnke**[4], **Naoum P. Issa**[#3], **Wim van Drongelen**[#1,2,3,5,*]

[1]Department of Pediatrics, The University of Chicago, Chicago, IL, 60607, USA

[2]Committee on Neurobiology, The University of Chicago, Chicago, IL, 60607, USA

[3]Department of Neurology, The University of Chicago, Chicago, IL, 60607, USA

[4]Department of Surgery, The University of Chicago, Chicago, IL, 60607, USA

[5]Committee on Computational Neuroscience, The University of Chicago, Chicago, IL, 60607, USA

[#] These authors contributed equally to this work.

Abstract

Introduction: Epileptiform activity limited to deep sources such as the hippocampus currently lacks reliable scalp correlates. Recent studies, however, have found that a subset of hippocampal interictal discharges may be associated with visible scalp signals, suggesting that some types of hippocampal activity may be monitored noninvasively. The relationship between these scalp waveforms and the underlying intracranial activity remains to be studied.

Methods: Paired intracranial and scalp EEG recordings obtained from 16 patients were used to identify hippocampal interictal discharges. Discharges were grouped by waveform shape, and spike-triggered-averages (STA) of the intracranial and scalp signals were calculated for each group. Cross-correlation of intracranial and scalp STAs was used to determine their temporal relationship, and topographic maps of the scalp were generated for each group.

Results: Cross-correlation of intracranial and scalp correlates resulted in two classes of scalp waveforms—those with and without time delays from the associated hippocampal discharges. Scalp signals with no delay showed topographies with a broad field with higher amplitudes on the side ipsilateral to the discharges and a left-right flip in polarity—observations consistent with the volume conduction of a single unilateral deep source. In contrast, scalp correlates with time lags showed rotational dynamics, suggesting synaptic propagation mechanisms.

Conclusions: The temporal relationship between the intracranial and scalp signals suggests that both volume conduction and synaptic propagation contribute to these scalp manifestations.

[*]**Corresponding Author:** Wim van Drongelen, 5841 South Maryland Avenue, MC 6082, Chicago, IL 60637, (T) 773-834-9049, wvandron@peds.bsd.uchicago.edu.

AUTHOR CONTRIBUTIONS

Data collection: SW, JT, SR, PW, NI. Study design: SL, NI, WvD, SW. Data analysis: SL. All authors contributed to writing and editing of this manuscript.

Conflict of Interest: The authors declare that the research was conducted in the absence of any commercial or financial relationships that could be construed as a potential conflict of interest.

Furthermore, the topographic evolution of these scalp waveforms may be used to distinguish spikes that are limited to the hippocampus from those that travel to or engage other brain areas.

Keywords

Hippocampus; interictal discharge; EEG; spike-triggered average; cross-correlation

INTRODUCTION

Mesial temporal lobe epilepsy (MTLE) is the most common form of focal epilepsy in adults, comprising over a quarter of all epilepsy cases [1, 2]. Despite its prevalence, MTLE is difficult to diagnose because hippocampal epileptiform activity is not readily identifiable on scalp electroencephalography (EEG) [3, 4]. Previously, a quantitative study showed that hippocampal spikes produce on average 7μV deflections on scalp EEG, making them difficult to distinguish from background fluctuations of ~10μV, leading to the conclusion that hippocampal discharges can generate clinically detectable signals on scalp recordings only with the engagement of an extended neocortical network [3]. In early MTLE, however, epileptiform activity may be restricted to the hippocampus, and the development of scalp EEG methods for detecting signals from deep brain sources is important for early diagnosis [5, 6], prevention of misdiagnoses [7], and reducing delay in getting definitive treatment [8, 9].

In contrast, some theoretical studies have argued that deep discharges might be detectable by both EEG and magnetoencephalography (MEG) [10, 11]. This theoretical finding was recently corroborated by a study demonstrating that individual hippocampal discharges can sometimes be detected by MEG [12]. In a clinical study, a subset of intracranially recorded hippocampal discharges were associated with waveforms visible on scalp EEG [13]. This study, however, could not preclude the possibility that the scalp waveforms were reflective of epileptiform activity that also engaged neocortical areas outside the hippocampus. In this study, we show that hippocampal discharges can manifest on scalp EEG recordings and result in distinct scalp topographical patterns that may allow inference of the nature of the underlying intracranial activity.

MATERIALS AND METHODS

Patients and Data Acquisition

Data were collected from 16 patients (Table 1) undergoing phase II monitoring for medically intractable right temporal lobe epilepsy between 2015 and 2017 at the University of Chicago Adult Epilepsy Center. Written informed consent was provided through a process approved by the University of Chicago Institutional Review Board.

All patients were implanted with a 12-channel depth electrode placed along the length of the right hippocampus through burr holes, with contact #1 (RHD1) being most anterior and contact #12 (RHD12) being most posterior [13]. Scalp EEG data collected from 22 electrodes (following international 10–10 arrangement) were used for analysis: F9, T9, F7, T7, P7, F3, C3, P3, O1, Fz, Cz, Pz, Oz, F4, C4, P4, O2, F8, T8, P8, F10, T10. EEG signals

were collected using the XLTEK system (Natus, Pleasanton, CA, USA), passband filtered at 0.1–344Hz, digitized at 1024 samples/s, and referenced to the FCz electrode.

Data Analysis

For each patient, a two-hour EEG segment recorded during drowsiness and sleep was analyzed. A custom C^{++} routine was used to convert raw data into Matlab files. All other analyses and statistics were performed in Matlab (Matlab, Natick, MA, USA).

The relationship between intracranial and extracranial signals was analyzed as follows:

1. Automated detection of intracranially recorded hippocampal discharges.
2. Grouping of similarly shaped hippocampal discharges using connected components analysis.
3. Calculation of spike-triggered averages (STAs) of intracranial and scalp EEG signals.
4. Cross-correlation of intracranial and scalp EEG signals
5. Topographic analysis of scalp signals.

Unless otherwise noted, the average reference montage was used, in which all signals were referenced to the average of the scalp EEG channels. All analyses were performed separately for each patient. Specifics of these five steps are described below.

(1) Detection of hippocampal discharges—Signals from the 12 channels on the right hippocampal depth (RHD) electrode were used to identify epochs containing interictal discharges. Because the detection method only utilized intracranial channels, the FCz common reference montage was used. EEG signals were digitally filtered using a zero-phase 2^{nd} order 10–50Hz Butterworth bandpass filter. The signals from the 12 RHD channels were then averaged, and peak detection was applied. Peaks were defined as points having an absolute amplitude >5 standard deviations from the signal mean and that were a local minimum or maximum in a 1 second window. This detection method was independently validated by visual inspection by an epileptologist (NPI).

(2) Grouping of hippocampal discharges—Hippocampal discharges in a given subject were grouped by waveform using connected component analysis [14]. A 500ms epoch centered on each peak was used for classification. For each epoch, signals from the 12 RHD channels were concatenated, creating a 6000 ms-long vector. A correlation coefficient was then calculated between pairs of vectors, resulting in an $n \times n$ correlation matrix where n was the number of hippocampal discharges. Using a correlation coefficient threshold (see below), this correlation matrix was converted into a binary matrix by replacing coefficients above or below the threshold with 1's and 0's, respectively. This binary matrix was then converted into an undirected graph in which discharges were represented by nodes connected by edges specified by 1's in the matrix. The connected components of this graph were extracted using the Matlab function *conncomp*, which assigns two nodes to the same component if they are connected by an edge. A group was defined as the set of discharges belonging to the same connected component.

To determine the appropriate threshold correlation coefficient for the grouping procedure, discharges were preliminarily grouped using threshold values ranging from 0.5 to 1.0 in 0.01 increments. The threshold value that maximized the number of large groups (defined as ≥20 discharges/group) was used in the final analysis (Supplementary Figure 1). This threshold value was determined for each patient separately.

(3) Calculation of spike-triggered averages for EEG signals—For each group of discharges, spike-triggered averages (STAs) for RHD and scalp EEG signals were calculated (Figures 1 & 2). STAs were calculated by averaging the signals from all discharges in a given group, using the peaks detected in the RHD signals as triggers. Noise levels were estimated using 250ms flanks before and after the 500ms STA epoch. The signal-to-noise ratio (*SNR*) in dB was defined as:

$$SNR = 20\log_{10}\left(\frac{RMS_{signal}}{RMS_{noise}}\right) \quad (1)$$

where RMS_{signal} is the root mean square (RMS) amplitude of the STA and RMS_{noise} is the RMS amplitude of the 250ms flanks around the STA. Scalp STAs with an SNR≥6dB were used for subsequent analyses.

(4) Cross-correlation of intracranial and scalp EEG signals—We determined the temporal relationship between the hippocampal discharge measured by the intracranial channels and the voltage changes measured by the scalp electrodes. Within each group of hippocampal discharges, we computed the cross-correlation R_{xy} between the intracranial channel STA with the highest amplitude (x) and scalp STAs at each electrode (y) using:

$$R_{xy}[k] = \sum_{m=1}^{N} x[m]y[m-k] \quad (2)$$

in which m is the index of the sampled data point, N is the total number of samples in the epoch, and k is the lag time. This procedure resulted in 22 cross-correlograms per group (Figure 3). For each cross-correlogram, the lag time at which the greatest absolute correlation occurred was determined.

Although volume conduction theoretically occurs with zero lag, noise in real recordings may cause the peak in cross-correlations of synchronous signals to deviate from zero. To determine what range of lag times is sufficiently small to be interpreted as zero, we conducted the following Monte Carlo simulation. We generated two 500ms epochs containing identical 20Hz sine waves: one epoch represented the intracranial hippocampal discharge and the other represented the scalp EEG signal. After various levels of random Gaussian noise were added to each epoch, the two epochs were cross-correlated, and the lag time at which the maximum correlation occurred was determined. The SNR for the epoch representing the intracranial signal was fixed at 25dB (a level based on our measurements), while a range of 6–25dB was used for the epoch representing the scalp signal. This procedure was repeated 1000 times for each noise level to generate a distribution of maximum correlation lag times for a range of SNRs. The 99% CI for this distribution was

determined, and lag times within this interval were considered to be sufficiently small to be interpreted as having no delay.

(5) Topographic analysis of scalp signals—For each discharge group, the scalp STAs were used to create field potential maps using EEGLAB software [15], using the *topoplot* function with default electrode coordinates. Topographic maps were generated for each time point across the 500ms STA epoch. The topographic maps reflect 2-dimensional projections of 3-dimensional coordinates of the scalp electrodes.

The dynamics of the scalp topography were quantified by the standard deviation (SD) in the direction of the scalp field dipole during the course of the 500ms discharge epoch. For each time point, the direction of the scalp field dipole was estimated by the angle between the inion-nasion line and the line connecting the electrodes with the minimum and maximum amplitude (Figure 4B). The dipole angle was calculated at time points with a dipole amplitude ≥5 standard deviations from the mean dipole amplitude over the 500ms epoch. To obtain reliable SD estimates, we only included groups that had scalp EEG SNR ≥6dB in at least 5 channels and waveforms with a minimum duration of 20ms.

RESULTS

Hippocampal interictal discharges were recorded on intracranial electrodes in 16 patients, and discharges from individual subjects were grouped based on morphological similarity. Across the 16 patients, 42 groups of hippocampal discharges were found. Figure 1A shows example STA signals from hippocampal depth electrodes for the five groups of discharges found in Patient 1 (Figure 1B). In groups 1, 2, 3, and 5, scalp EEG amplitudes were larger on the temporal channels ipsilateral to the spiking hippocampus and were inverted in polarity on the left temporal channels. Group 4, which had the smallest intracranial signals (Figure 1A), also showed the smallest scalp signals with maximal amplitudes in frontal channels (Figure 1B). Scalp EEG amplitudes ranged between 1 and 19μV with an average±standard deviation of 5.5±4.1μV (N=42 groups; Figure 2).

Characterization of scalp waveforms based on temporal lag from hippocampal discharges

Next, we asked if the scalp EEG patterns could be generated by volume conduction of hippocampal discharges. Volume conduction occurs at the speed of light, so a finding of no lag between a scalp signal and an associated hippocampal discharge would be consistent with volume conduction. Temporal lag was determined from the cross-correlogram between each scalp EEG channel STA and the depth electrode channel STA with the greatest amplitude (Figure 3A). For example, in Group 1, cross-correlation of the STA of scalp channel F9 and the STA of channel RHD4 yielded a maximum correlation coefficient of 0.93 at a lag time of −3ms, where a negative value implies the scalp signal leads the hippocampal signal.

Although volume conduction theoretically occurs with zero lag, noise in real recordings may cause the peak in cross-correlations of synchronous signals to deviate from zero. To determine the range of measured lag times that were sufficiently small to be interpreted as zero, we conducted a Monte Carlo simulation of lag times resulting from cross-correlation

of two identical signals corrupted by varying levels of noise (Methods). The black curve in Figure 3B shows the result of this simulation and represents the 99% confidence interval (CI) for the distribution of lag times across the range of signal to noise ratios (SNR). For example, for the cross-correlation of an 8dB scalp signal with a 25dB hippocampal signal, the 99% CI of lag times was ±4.8ms. As expected, signals with low SNR have a larger spread of lag times than signals with high SNR. This non-zero threshold for lag times does allow for the possibility of physiological propagation in waveforms categorized as volume conduction. Consequently, we interpret small lag times *not as proof* of volume conduction, but rather a characteristic that is *consistent* with volume conduction.

The scatter plot in Figure 3B shows the lag times of all scalp channel STAs for Patient 1. Points that fall below the 99% CI line have a lag sufficiently close to zero to be consistent with volume conduction. For points that fall above the simulation curve, scenarios involving secondary sources likely contribute to the scalp signal. Of the 5 groups identified, Group 4 had the smallest amplitude signals in both the hippocampal and scalp channels. The small and sparse nature of the scalp signals seen in Group 4 reduces their interpretability, and therefore we highlight here the results of other groups with more robust and distinctive characteristics. Of the 20 channels with significant scalp signals in Group 2, 16 channels had lag times below the 99% CI while 4 channels had lag times above. This observation suggests that the scalp correlates seen for Group 2 are more consistent with volume conduction. In contrast, Group 5 had 21 channels with significant scalp signals, 17 of which had lag times greater than the 99% CI, suggesting that the scalp correlates for Group 5 are more consistent with a secondary source.

Topographic analysis of scalp STAs

In addition to temporal correlation, we investigated the spatio-temporal development of scalp discharges. We hypothesized that scalp topographies that reflect volume conduction from a single deep source would exhibit a relatively stationary dipole, while sources that propagate to and engage other brain areas would show a more dynamic evolution of scalp potentials. The scalp STAs for each group were used to generate topographic maps of scalp potentials at different time points. The topographies for the five groups from Patient 1 are shown in Figure 4A. Qualitatively, some of the discharges show fields that are largely stationary except for an abrupt flip in polarity (e.g. Figure 4A, Group 2), while others show a more dynamic, rotational pattern (e.g. Figure 4A, Group 5). To quantify this observation, we used the standard deviation (SD) in the field dipole angle as a metric to determine how the topography of each discharge evolves over time (Methods, Figure 4B). Of the 42 groups, 24 met criterion for inclusion in this analysis (Methods). Small angle-SD implied a relatively stationary dipole, while a high angle variance implied a rotating dipole. We then asked if the SD of this angle correlated with the percentage of scalp channels with no lag in that group (Figure 4C). The groups dominated by zero lag times showed smaller SD (i.e. more stationary topographies) than groups with predominantly non-zero lag times ($r = -0.61$; $p = 0.001$). This supports the hypothesis that scalp manifestations consistent with volume conduction are more stationary than discharges consistent with other mechanisms such as neuronal propagation.

DISCUSSION

In this study, we present evidence that scalp waveforms associated with hippocampal interictal discharges have various topographic morphologies. Furthermore, whether the scalp waveform was consistent with volume conduction of a hippocampus-limited discharge could be determined by comparing the lag time between the scalp and hippocampal signals.

Two types of scalp topography were identified—static and dynamic. In the static case, electrical fields were consistent with a largely stationary dipole with an abrupt left-right flip during the course of the discharge. These characteristics, along with the observations that waveforms were present bilaterally with higher amplitudes on the side ipsilateral to the hippocampal spike and with inverted polarity on the contralateral scalp electrodes, point to a lateralized, single, deep source. Additionally, the near-simultaneous timing of the scalp and hippocampal waveforms and the high correlations between their waveforms are consistent with a signal that travels from the hippocampus to the scalp via volume conduction, an electromagnetic process that occurs with virtually zero delay. In contrast, scalp waveforms that occur with significant lag from the hippocampal discharge showed more complex, rotational dynamics, with lower correlations between the scalp and hippocampal discharge waveforms, suggestive of a signal that either travels to or engages other cortical areas using a more time-consuming mechanism such as neuronal propagation and synaptic transmission (Figures 3 & 4). Some waveforms showed significant negative lag times, meaning that the scalp signal precedes the hippocampal signal. This suggests that the scalp electrode was reflecting activity that occurred in a different brain area or propagated *to* the hippocampus. By using only hippocampal depth and scalp electrodes, it is not possible to ascertain the exact origin of physiologically propagated signals. This limitation may be addressed in future studies that incorporate recordings from other brain areas.

Other groups have suggested that differences in topographic evolution can be used to differentiate between benign and pathological scalp small sharp spikes [16]. Both the static and dynamic waveforms observed in our study show a horizontal dipole at the time of the spike, consistent with what has been described as benign epileptiform transients of sleep (BETS) [16]. However, BETS showed a 30° rotational component, suggesting that our dynamic group aligns more with what has been described as BETS while our static group may be more aligned with pathological waveforms [17]. To differentiate between benign versus pathological waveforms, more comprehensive prospective studies using both neurotypical and epileptic patients will be required.

In mesial temporal lobe epilepsy, epileptiform activity can be limited to deep structures such as the hippocampus or involve larger networks that include neocortical regions. Classical epileptiform discharges such as spikes and sharp waves are frequently observed on scalp EEG when neocortical regions are involved [3, 18]. When epileptiform activity is restricted to regions around the hippocampus, however, scalp waveforms are not readily apparent [4], and only small sharp spikes have been implicated as scalp EEG markers of hippocampal discharges [13]. While the natural history of temporal lobe epilepsy is incompletely defined [19, 20, 21, 22], one line of thought posits that epileptogenic activity is restricted to the hippocampus in the early phases of MTLE with recruitment of neocortex occurring as the

disease progresses [23, 24, 25]. Because engagement of larger networks may be associated with poorer surgical outcomes with targeted resections [26], the ability to detect and differentiate early hippocampal discharges with or without neocortical involvement could lead to earlier diagnosis, preventing misdiagnoses, and improving patient outcomes.

One important limitation in this study is that intracranial recordings from patients were limited to 12-channels on hippocampal depth electrodes. The exact source of a scalp signal cannot be definitively proven without sampling from many brain areas simultaneously. However, the combination cross-correlation lag times and scalp signal topography can be used to categorize hippocampal spikes into those consistent with physiological propagation and those consistent with volume conduction. A definitive localization of all discharge sources, especially those consistent neuronal propagation, will depend on intracranial source localization methods that rely on electrodes in addition to hippocampal depth channels.

For clinical purposes, hippocampal discharges in early MTLE should ideally be identifiable without the need for invasive monitoring. Scalp markers are likely to be low in sensitivity for the detection of individual hippocampal discharges since we are relying on greatly attenuated hippocampal signals to break through the relatively high noise levels of the scalp EEG. Chen et al. found that in patients evaluated in an epilepsy monitoring unit, small sharp spikes on scalp EEG had an odds ratio of 9.1 for epilepsy, but only a sensitivity of ~19% [27]. In our own dataset, approximately 15% of all hippocampal spikes were associated with a visible waveform on the scalp, results that are within range with the detection rate of 22% found by down-sampling dense array scalp EEG signals [28]. Although sensitivity for individual hippocampal discharges is low, small sharp spikes may be visible in up to 50% of patients with hippocampal discharges [13]. If indeed some of these waveforms are a result of volume conduction of hippocampal discharges, higher rates of detection may be possible for patients with smaller heads and thinner bone, meaning that this may be a particularly useful marker in pediatric populations. For example, children with febrile status epilepticus have been shown to be at higher risk for developing TLE [29], and small sharp spikes might be an early marker for such pathology.

Supplementary Material

Refer to Web version on PubMed Central for supplementary material.

ACKNOWLEDGEMENTS

We thank Graham Smith and Dr. Vernon L. Towle for valuable discussion and input to the manuscript.

FUNDING

This work was supported by NIH Grants R01 NS095368 (WvD), R01 NS084142 (WvD and SL), R01 NS116262 (NPI), and the University of Chicago MSTP Training Grant T32GM007281

Data Availability Statement:

All code used for statistical analysis and signal processing is available upon request

REFERENCES

1. Asadi-Pooya AA, Stewart GR, Abrams DJ, & Sharan A (2016). Prevalence and incidence of drug-resistant mesial temporal lobe epilepsy in the United States. World Neurosurgery. 10.1016/j.wneu.2016.12.074
2. Stern J, & Engel J Jr. (2015). Mesial temporal lobe epilepsy with hippocampal sclerosis. Retrieved April 1, 2016, from http://www.medlink.com/article/mesial_temporal_lobe_epilepsy_with_hippocampal_sclerosis
3. Koessler L, Cecchin T, Colnat-Coulbois S, Vignal J-P, Jonas J, Vespignani H, … Maillard LG (2015). Catching the Invisible: Mesial Temporal Source Contribution to Simultaneous EEG and SEEG Recordings. Brain Topography, 28(1), 5–20. 10.1007/s10548-014-0417-z [PubMed: 25432598]
4. Wennberg R, Valiante T, & Cheyne D (2011). EEG and MEG in mesial temporal lobe epilepsy: where do the spikes really come from? Clinical Neurophysiology : Official Journal of the International Federation of Clinical Neurophysiology, 122(7), 1295–1313. 10.1016/j.clinph.2010.11.019 [PubMed: 21292549]
5. Jacoby A, Baker GA, Steen N, Potts P, & Chadwick DW (1996). The Clinical Course of Epilepsy and Its Psychosocial Correlates: Findings from a U.K. Community Study. Epilepsia, 37(2), 148–161. 10.1111/j.1528-1157.1996.tb00006.x [PubMed: 8635425]
6. Sperling MR (2004). The consequences of uncontrolled epilepsy. CNS Spectrums, 9(2), 98–101, 106–109. Retrieved from http://www.ncbi.nlm.nih.gov/pubmed/14999166 [PubMed: 14999166]
7. Mirsattari SM, Gofton TE, & Chong DJ (2011). Misdiagnosis of epileptic seizures as manifestations of psychiatric illnesses. The Canadian Journal of Neurological Sciences. Le Journal Canadien Des Sciences Neurologiques, 38(3), 487–493. Retrieved from http://www.ncbi.nlm.nih.gov/pubmed/21515510 [PubMed: 21515510]
8. Berg AT (2004). Understanding the delay before epilepsy surgery: who develops intractable focal epilepsy and when? CNS Spectrums, 9(2), 136–144. Retrieved from http://www.ncbi.nlm.nih.gov/pubmed/14999169 [PubMed: 14999169]
9. Simonato M, Löscher W, Cole AJ, Dudek FE, Engel J, Kaminski RM, … Klitgaard H (2012). Finding a better drug for epilepsy: preclinical screening strategies and experimental trial design. Epilepsia, 53(11), 1860–1867. 10.1111/j.1528-1167.2012.03541.x [PubMed: 22708847]
10. Attal Y, Bhattacharjee M, Yelnik J, Cottereau B, Lefevre J, Okada Y, … Baillet S (2007). Modeling and Detecting Deep Brain Activity with MEG & EEG. In 2007 29th Annual International Conference of the IEEE Engineering in Medicine and Biology Society (pp. 4937–4940). IEEE. 10.1109/IEMBS.2007.4353448
11. Goldenholz DM, Ahlfors SP, Hämäläinen MS, Sharon D, Ishitobi M, Vaina LM, & Stufflebeam SM (2009). Mapping the signal-to-noise-ratios of cortical sources in magnetoencephalography and electroencephalography. Human Brain Mapping, 30(4), 1077–1086. 10.1002/hbm.20571 [PubMed: 18465745]
12. Pizzo F, Roehri N, Medina Villalon S, Trébuchon A, Chen S, Lagarde S, … Bénar CG (2019). Deep brain activities can be detected with magnetoencephalography. Nature Communications, 10(1), 971. 10.1038/s41467-019-08665-5
13. Issa NP, Wu S, Rose S, Towle VL, Warnke PC, & Tao JX (2018). Small sharp spikes as EEG markers of mesiotemporal lobe epilepsy. Clinical Neurophysiology, 129(9), 1796–1803. 10.1016/J.CLINPH.2018.06.011 [PubMed: 30005212]
14. Hopcroft J, & Tarjan R (1973). Algorithm 447: efficient algorithms for graph manipulation. Communications of the ACM, 16(6), 372–78. 10.1145/362248.362272
15. Delorme A, & Makeig S (2004). EEGLAB: an open source toolbox for analysis of single-trial EEG dynamics including independent component analysis. Journal of Neuroscience Methods (Vol. 134). Retrieved from http://www.sccn.ucsd.edu/eeglab/
16. Wennberg R, Tarazi A, & Zumsteg D (2018). Which small sharp spikes are benign epileptiform transients of sleep? Clinical Neurophysiology.

17. Issa NP, Lee S, Wu S, Rose S, Towle VL, Warnke PC, … Tao JX (2018). Reply to "Which small sharp spikes are benign epileptiform transients of sleep?" Clinical Neurophysiology, 0(0). 10.1016/j.clinph.2018.09.002

18. Merlet I, & Gotman J (1999). Reliability of dipole models of epileptic spikes. Clinical Neurophysiology, 110(6), 1013–1028. 10.1016/S1388-2457(98)00062-5 [PubMed: 10402088]

19. Berg AT (2008). The natural history of mesial temporal lobe epilepsy. Current Opinion in Neurology, 21(2), 173–178. 10.1097/WCO.0b013e3282f36ccd [PubMed: 18317276]

20. Hesdorffer DC, Shinnar S, Lax DN, Pellock JM, Nordli DR, Seinfeld S, … FEBSTAT study team S (2016). Risk factors for subsequent febrile seizures in the FEBSTAT study. Epilepsia, 57(7), 1042–1047. 10.1111/epi.13418 [PubMed: 27265870]

21. Issa NP, Sedler MJ, Del Brutto VJ, Darsan E, Milla L, Montes J, … Del Brutto OH (2018). EEG Patterns in Patients With Calcified Neurocysticercosis With or Without Hippocampal Atrophy. Journal of Clinical Neurophysiology, 35(4), 332–338. 10.1097/WNP.0000000000000471 [PubMed: 29649013]

22. Shukla G, & Prasad AN (2012). Natural history of temporal lobe epilepsy: antecedents and progression. Epilepsy Research and Treatment, 2012, 195073. 10.1155/2012/195073 [PubMed: 22937237]

23. Morrell F (1985). Secondary epileptogenesis in man. Arch. Neurol, 42(4), 318–35. 10.1001/archneur.1985.04060040028009. [PubMed: 3921008]

24. Morrell F (1989). Varieties of human secondary epileptogenesis. J Clin Neurophysiol Jul;6(3):227–75. 10.1097/00004691-198907000-00002. [PubMed: 2503538]

25. Wennberg R, Quesney F, Olivier A, & Dubeau F (1997). Mesial temporal versus lateral temporal interictal epileptiform activity: comparison of chronic and acute intracranial recordings. Electroencephalogr. Clin. Neurophysiol Jun;102(6):486–94. 10.1016/s0013-4694(97)96018-5. [PubMed: 9216481]

26. Sinha N, Dauwels J, Kaiser M, Cash SS, Brandon Westover M, Wang Y, & Taylor PN (2017). Predicting neurosurgical outcomes in focal epilepsy patients using computational modelling. Brain : A Journal of Neurology, 140(2), 319–332. 10.1093/brain/aww299 [PubMed: 28011454]

27. Chen Z, Issa NP, Wu S, Liu X, Sun T, Bodnya J, Rose S, Tao JX (2020). The clinical significance of small sharp spikes: A retrospective study of 909 patients in epilepsy monitoring unit. Epilepsy Res Dec;168:106477. 10.1016/j.eplepsyres.2020.106477. Epub 2020 Oct 5. [PubMed: 33096313]

28. Yamazaki M, Tucker DM, Fujimoto A, Yamazoe T, Okanishi T, Yokota T, … Yamamoto T (2012). Comparison of dense array EEG with simultaneous intracranial EEG for Interictal spike detection and localization. Epilepsy Research, 98(2–3), 166–173. 10.1016/J.EPLEPSYRES.2011.09.007 [PubMed: 22018998]

29. Lewis DV, Shinnar S, Hesdorffer DC, Bagiella E, Bello JA, Chan S, Xu Y, MacFall J, Gomes WA, Moshé SL, Mathern GW, Pellock JM, Nordli DR Jr., Frank LM, Provenzale J, Shinnar RC, Epstein LG, Masur D, Litherland C, Sun S; FEBSTAT Study Team. Hippocampal sclerosis after febrile status epilepticus: the FEBSTAT study. Ann Neurol 2014 Feb;75(2):178–85. 10.1002/ana.24081. [PubMed: 24318290]

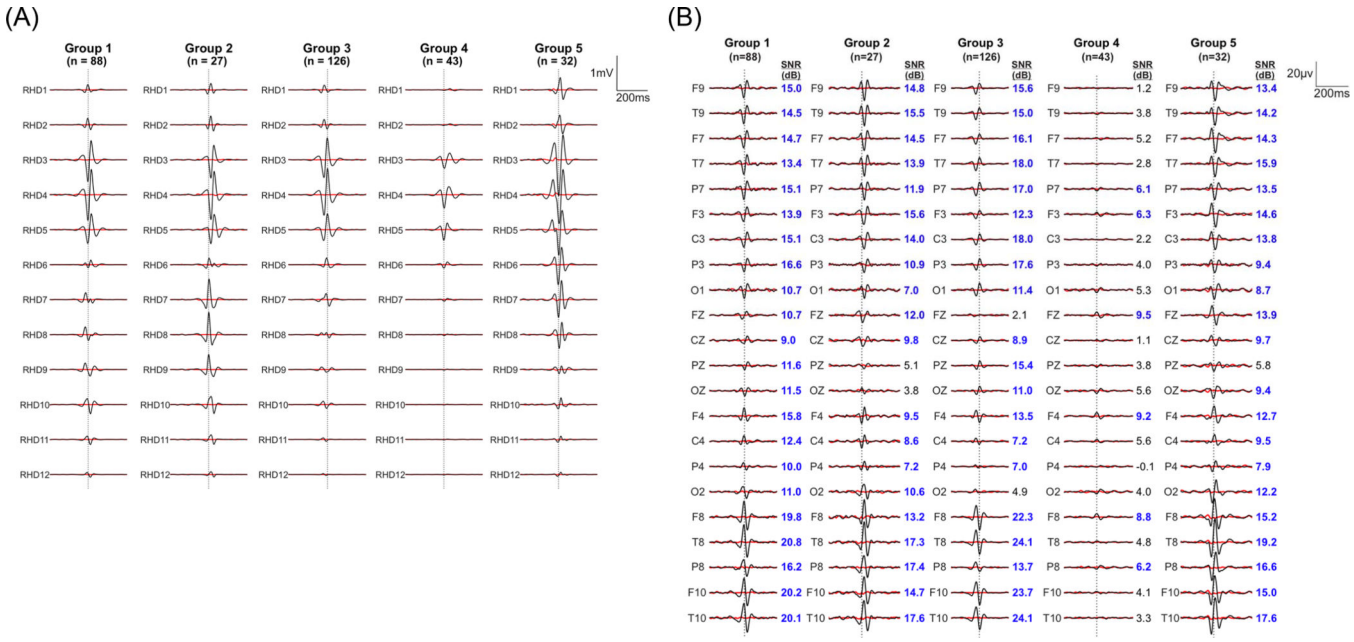

Figure 1:

Spike triggered averages (STAs) for the hippocampal discharges in the five groups of Patient 1. Black traces are the STAs and the red traces show the associated noise estimates. Noise was estimated in the 250ms epochs before and after the discharge epoch of 500ms. (A) STAs of intracranial channels. The depth electrode label is indicated for each waveform. RHD = right hippocampal depth electrode. RHD1 is the most anterior contact, and RHD12 is the most posterior contact. (B) STAs of scalp EEG channels. The electrode location and the SNR (dB) are indicated left and right for each waveform. SNR values greater than 6dB are denoted in blue.

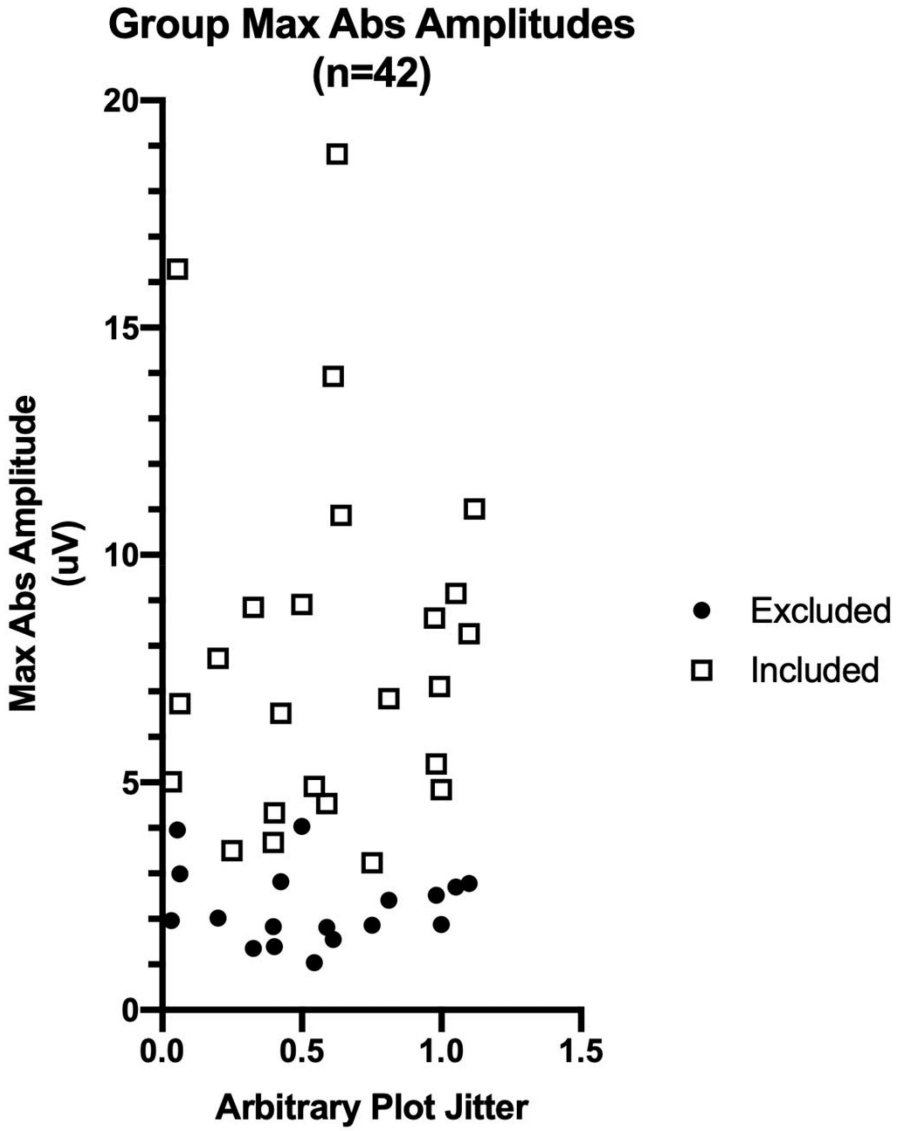

Figure 2.

Distribution of maximum absolute scalp STA amplitudes by group. For each of the 42 groups of hippocampal discharges, the greatest absolute amplitude seen across all channels in the scalp signal STA is plotted. Symbol shapes indicate groups included or excluded from the analysis shown in Figure 4c.

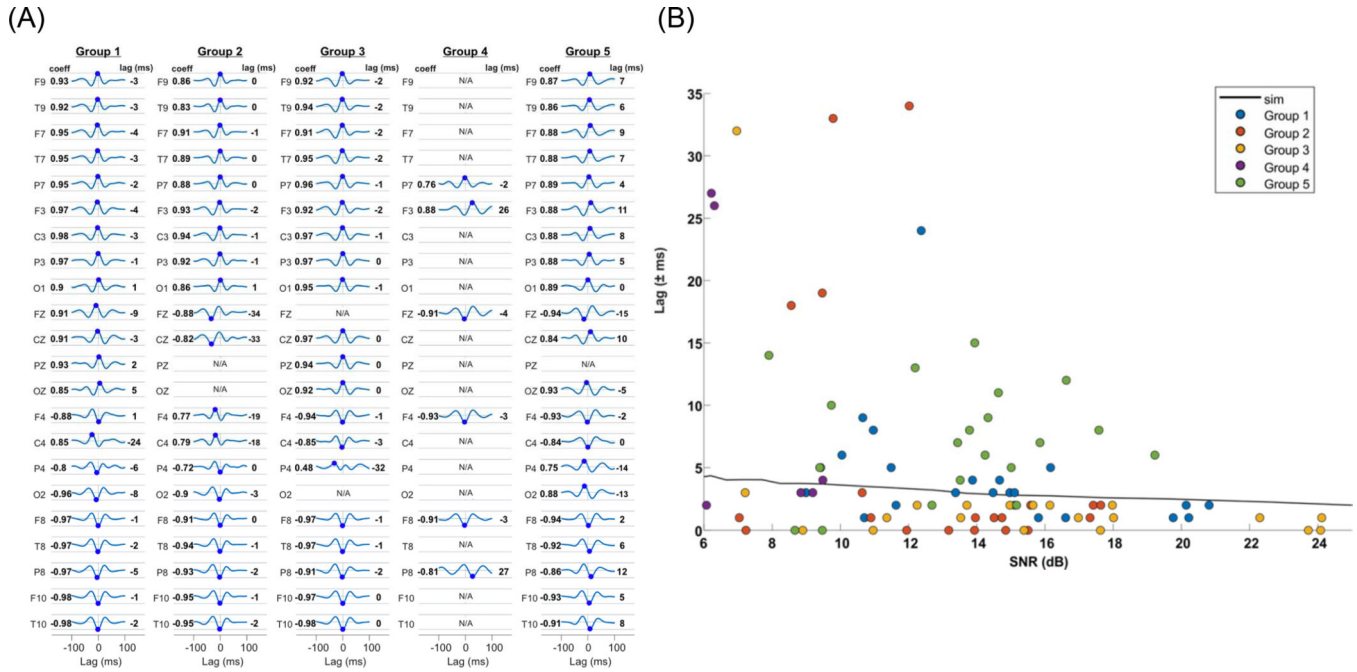

Figure 3:

Cross-correlation analysis of intracranial and scalp EEG STAs of hippocampal discharges. (A) Cross-correlograms for Patient 1. Cross-correlation was determined between the largest hippocampal signal in Figure 1A and its associated scalp waveforms depicted in Figure 1B. Correlation values are scaled between ±1 (grey horizontal lines) and the lags are computed between ±100ms. For each scalp electrode, the greatest absolute correlation coefficient and its lag (ms) are written on the left and right, respectively, for each waveform. The greatest absolute correlation coefficient for each correlogram is indicated by the blue dot. (B) Determining scalp channels with lags consistent with volume conduction of a hippocampal source. Scatterplot of lags plotted versus the SNR of the five groups of Patient 1. The solid line indicates the simulated 99% confidence for zero lag corrupted by noise (Methods). Note that for groups 2 and 3 most channels are below the line while for group 5 most are situated above the line.

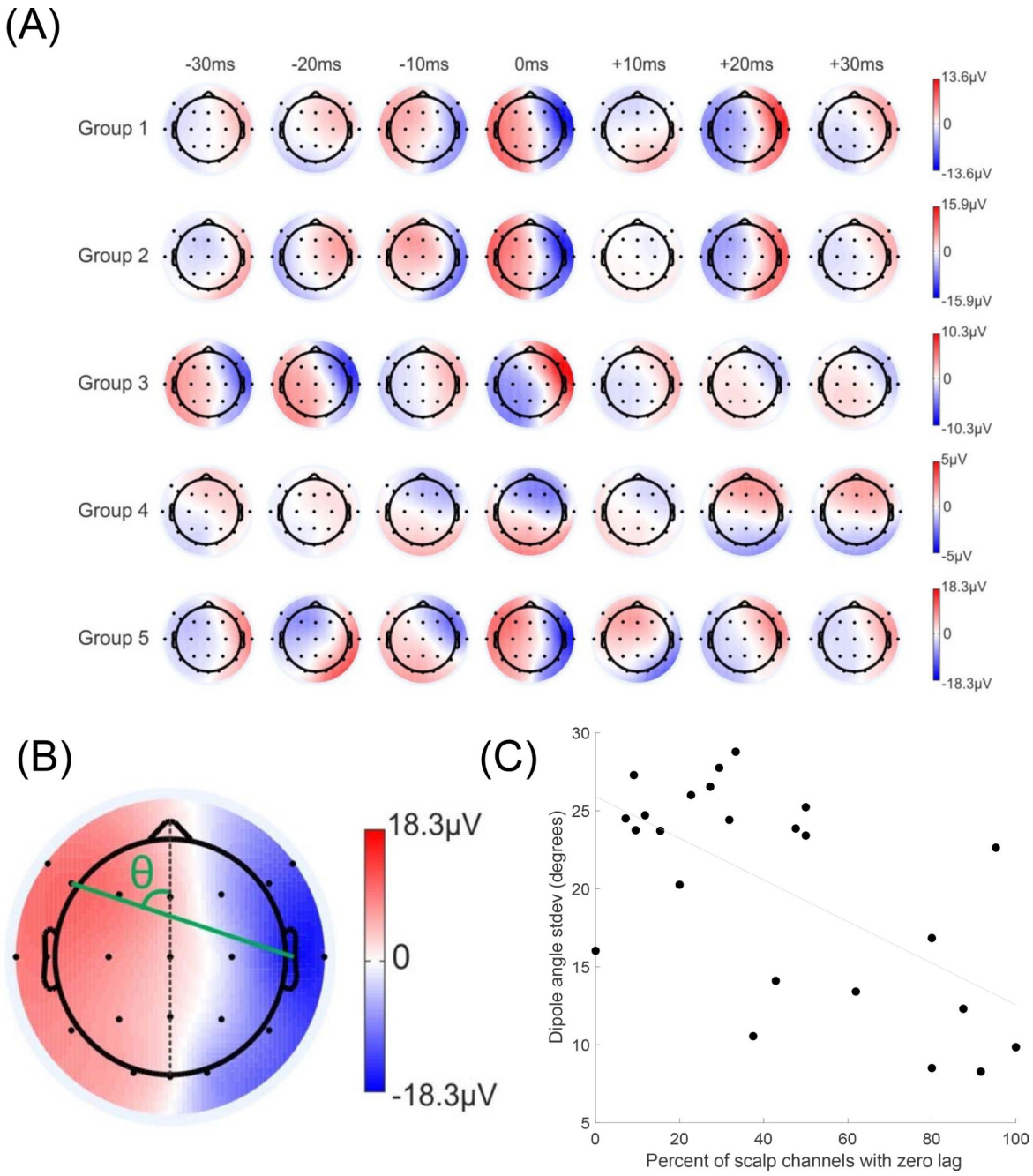

Figure 4:

Topographic analysis of hippocampal discharge-related scalp EEG signals. (A) Topography of the five groups of discharges in Patient 1. The zero value of the time scale is aligned with the maximum amplitude of the discharge. (B) To estimate the angle of the dipole underlying the topographic field, a line was drawn between the electrodes with the maximum and minimum value (green). The zero–degree axis was defined as the inion-nasion line (dotted black). (C) For all patients and groups: variance of topography plotted versus the % of channels with zero lag. The line is the linear regression ($n = 24$; r = −0.62, $p = 0.001$).

Table 1.

Summary of demographics and diagnosis for all 16 patients.

Patient #	Age	Gender	Diagnosis
1	51	Female	Right MTLE
2	21	Male	Bilateral MTLE
3	33	Male	Bilateral MTLE
4	51	Male	Bilateral MTLE
5	33	Female	Right MTLE
6	21	Male	Bilateral MTLE
7	22	Female	Right MTLE
8	22	Female	Bilateral MTLE
9	24	Male	Right MTLE
10	40	Female	Right MTLE
11	19	Female	Right MTLE
12	47	Female	Right MTLE
13	26	Male	Right MTLE
14	43	Male	Right MTLE
15	58	Female	Right MTLE
16	44	Female	Bilateral MTLE

MTLE = mesial temporal lobe epilepsy